Acta Cryst. (1997). A53, 168–174

Effects of the Elastic Stress Relaxation on the HRTEM Image Contrast of Strained Heterostructures

L. De Caro,[a]* A. Giuffrida,[b] E. Carlino[a] and L. Tapfer[a]

[a]*PASTIS-Centro Nazionale Ricerca e Sviluppo Materiali (PASTIS-CNRSM), Strada Statale 7 Appia km 712, I-72100 Brindisi, Italy, and* [b]*Istituto Nuovi Materiali per l'Elettronica (CNR-IME), c/o Università degli Studi di Lecce, via Arnesano, I-73100 Lecce, Italy. E-mail: decaro@cnrsm.it*

(Received 15 July 1996; accepted 4 October 1996)

Abstract

In this work, the effects of the elastic relaxation of compositional stresses caused by the finite size of transmission electron microscopy (TEM) specimens on the image contrast of high-resolution transmission electron microscopy (HRTEM) micrographs of strained heterostructures made by cubic materials are investigated. The reduced spatial dimensions, owing to the thinning process of strained heterostructures, cause modification of the atomic positions in the thinned specimens with respect to the bulk ones. This deformation is a function not only of the specimen thickness but also of the thinning crystallographic direction. The results show that the strains of an elastically relaxed structure can vary by 15% as a function of the thinning direction ([100] or [011]). The bending of the atomic columns caused by the elastic relaxation phenomena in HRTEM specimens of strained semiconductor materials can cause a strong background-intensity variation in the HRTEM images. This effect is a function of the structure of the investigated materials, indicating that information on the background intensity variation, owing to the non-uniform lattice distortion of an elastically relaxed heterostructure made by cubic materials, is contained in the {200} beams. Thus, the influence of the elastic relaxation cannot be neglected whenever HRTEM is used to deduce the local chemical composition or the local unit cell in strained cubic materials.

1. Introduction

An accurate quantitative and spatially resolved structural characterization of heterostructures is very important because the atomic configuration of the heterointerfaces and the strain status of the heterostructures play an important role in the physical properties of a large class of materials (see, for example, Vandenberg, Macrander, Hamm & Panish, 1991; Hybertsen, 1990, 1991).

One of the most suitable techniques for structural characterization is transmission electron microscopy (TEM). In particular, high-resolution transmission electron microscopy (HRTEM) represents a powerful tool to investigate the structural status of heterointerfaces (Spence, 1981). HRTEM micrograph features are related to a variety of causes, such as specimen structure, composition and thickness, surface contamination, ion-milling damage, elastic stress relaxation and actual values of the electro-optical parameters. Consequently, quantitative structural near atomic resolution information is quite difficult to achieve.

The present work concerns elastic stress relaxation. In fact, owing to the very small thickness (1–30 nm) of HRTEM specimens, an elastic stress relaxation of strained heterostructures may occur near the free surfaces as a result of the reduced spatial dimensions introduced by the thinning process (Gibson & Treacy, 1984; Treacy, Gibson & Howie, 1985; Treacy & Gibson, 1986; Perovic, Weatherly & Houghton, 1988, 1991; De Caro, Giuffrida, Carlino & Tapfer, 1995). This relaxation phenomenon modifies the structural features of the thinned specimens with respect to the bulk materials. The local lattice spacings are representative of neither the bulk tetragonally distorted material nor the unstressed material (Gibson & Treacy, 1984; Treacy, Gibson & Howie, 1985; Treacy & Gibson, 1986; Perovic, Weatherly & Houghton, 1988, 1991; De Caro, Giuffrida, Carlino & Tapfer, 1995). Thus, the role of relaxation has to be taken into account whenever HRTEM is used to deduce the structural properties or the unit cell of the bulk heterostructures from those of the thinned specimens quantitatively.

In order to simulate the influence of the elastic relaxation on the HRTEM micrographs, the following steps should be considered: (i) strain status modeling for HRTEM specimens in the presence of elastic relaxation phenomena; (ii) implementation of computer programs to model the deformed heterostructures that are used to simulate the HRTEM images; it is worthwhile remarking that non-uniform strain fields involve thousands of atoms and, therefore, the supercells describing the characteristics of the deformed structure have to be properly dimensioned; (iii) computer implementation of suitable algorithms to extract the atomic positions of the

© 1997 International Union of Crystallography
Printed in Great Britain – all rights reserved

ISSN 0108-7673 © 1997

distorted crystalline lattice from the experimental and simulated HRTEM images for a more quantitative comparison with the theoretical predictions.

The first step has been already discussed (Gibson & Treacy, 1984; Treacy, Gibson & Howie, 1985; Treacy & Gibson, 1986; Perovic, Weatherly & Houghton, 1988, 1991) for TEM specimens of strained heterostructures thinned along the [100] crystallographic direction, and generalized for specimens thinned along the [110] crystallographic direction (De Caro, Giuffrida, Carlino & Tapfer, 1995; De Caro, Giuffrida & Tapfer, 1996). Step (ii) is the aim of the present work. In fact, we show how useful information can be achieved by comparing the contrast variation of the simulated HRTEM images with the experimental ones, taking into account the elastic stress relaxation.

We show that the non-uniform lattice distortion generated by the elastic stress relaxation of the thinned HRTEM specimens can cause for some crystallographic structures the presence of a strong background-intensity variation, overlapped to the 'phase contrast' of the HRTEM images. This contrast has been experimentally observed by Bierwolf, Hohenstein, Phillipp, Brandt, Crook & Ploog (1993) in HRTEM specimens of InAs quantum wells a few monolayers thick, bounded by GaAs barriers, and can be easily interpreted (erroneously) as due to chemical-composition gradients.

Moreover, this background-intensity variation caused by elastic relaxation is always visible for HRTEM specimens of lattice-mismatched III–V group semiconductor heterostructures (with a zinc blende crystallographic structure) but it is often negligible in HRTEM micrographs of IV–IV group semiconductor heterostructures (with a diamond crystallographic structure), independently of the lattice-mismatch value. This last finding demonstrates that the information on the background-intensity variation owing to the non-uniform lattice distortion of an elastically relaxed zinc blende heterostructure is contained in the {200} beams, forbidden for diamond-like crystallographic structures.

The paper is organized as follows: in §2, the theoretical model for the deformation fields in the presence of elastic relaxation of the compositional stresses of HRTEM specimens is reported. The specimens are considered to be made by cubic materials and to be thinned along the [110] or the [001] crystallographic direction; in §3, the results and discussion are reported; finally, conclusions are given in §4.

2. Strain-field calculation

Let us consider a strained superlattice of period T, grown along the $\mathbf{x} = [100]$ crystallographic direction and made of two cubic materials A and B with thicknesses a and b, and lattice parameters d_a and d_b, respectively. High-resolution transmission electron microscopy investigation requires specimen preparation involving a thinning process, which causes a finite size t along the thinning direction $\mathbf{z} = (1/2^{1/2})[011]$ (Fig. 1). The dimension of the superlattice can be considered infinite along the other orthogonal direction $\mathbf{y} = (1/2^{1/2})[01\bar{1}]$ (perpendicular to the plane of Fig. 1).

The strain and stress fields of the heterostructure here considered can be calculated following the Fourier-series elasticity treatment first introduced by Gibson & Treacy (1984) for the [100] thinning direction. The details of the calculations have been reported elsewhere (De Caro, Giuffrida & Tapfer, 1996). The total strains (elastic plus lattice-mismatch contributions) along the x and z axes are given by

$$\begin{aligned}
\varepsilon_{xx}^{\rm tot}(x,z) = \sum_p \varepsilon_p \cos(\alpha_p x)\big[[(C_{11}-C_{12})/C_{11}m^{1/2}]\\
\times (C_{11}+2C_{12})\big(\{2/[\beta_p \sin(\gamma_p t)\\
+ \gamma_p \sinh(\beta_p t)]\}[r_p \cosh(\beta_p z)\cos(\gamma_p z)\\
+ s_p \sinh(\beta_p z)\sin(\gamma_p z)] - S_{12}\{1\\
- [(S_{12}+S/2)/(S_{11}-S/2)]m^{1/2}\}\big)\\
- S_{12}/(S_{11}-S/2)\big],\\
\varepsilon_{zz}^{\rm tot}(x,z) = \sum_p \varepsilon_p \cos(\alpha_p x)\big[[(C_{11}-C_{12})/C_{11}m^{1/2}]\\
\times (C_{11}+2C_{12})\big(\{2/[\beta_p \sin(\gamma_p t)\\
+ \gamma_p \sinh(\beta_p t)]\}[u_p \cosh(\beta_p z)\cos(\gamma_p z)\\
+ v_p \sinh(\beta_p z)\sin(\gamma_p z)] - \{[S_{11}-S/2\\
- (S_{12}+S/2)^2/(S_{11}-S/2)]m^{1/2}\}\big)\\
+ (S_{12}+S/2)/(S_{11}-S/2)\big],
\end{aligned} \tag{1}$$

where, for the pth Fourier component,

$$\begin{aligned}
\varepsilon_p &= 2[T(d_a-d_b)/p\pi(ad_a+bd_b)]\sin(p\pi a/T),\\
\alpha_p &= 2p\pi/T,\\
\beta_p &= \alpha_p(2m^{1/2}+n)^{1/2}/2m^{1/2},\\
\gamma_p &= \alpha_p(2m^{1/2}-n)^{1/2}/2m^{1/2}.
\end{aligned} \tag{2}$$

Here, the C_{ij} and the S_{ij} are the stiffness and the compliance constants, respectively, and

$$\begin{aligned}
m &= (1+\alpha-2\nu)/2\alpha(1-\nu),\\
n &= [\alpha(1+\nu)+1-3\nu]/(1-\nu)
\end{aligned} \tag{3}$$

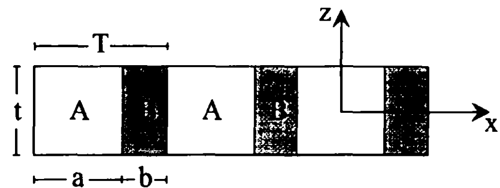

Fig. 1. Schematic view of a strained superlattice of period T made by two cubic semiconductor materials A and B with thicknesses a and b, respectively. t is the thickness of the TEM specimen in the thinning direction. The origin of the reference system is also shown.

are expressed as a function of the anisotropy coefficient $\alpha = (C_{11} - C_{12})/2C_{44}$ and the Poisson ratio $\nu = C_{12}/(C_{11} + C_{12})$.

Integrating (1), we obtain for the total atomic displacements along the x and the z axes, respectively:

$$\begin{aligned} s_x(x,z) &= \textstyle\int \varepsilon_{xx}^{\rm tot}(x,z)\,{\rm d}x \\ &= \sum_p \varepsilon_p \sin(\alpha_p x)[[(C_{11} - C_{12})/C_{11}m^{1/2}] \\ &\quad \times (C_{11} + 2C_{12})(\{2/[\beta_p \sin(\gamma_p t) + \gamma_p \sinh(\beta_p t)]\} \\ &\quad \times [r_p \cosh(\beta_p z)\cos(\gamma_p z) + s_p \sinh(\beta_p z) \\ &\quad \times \sin(\gamma_p z)] - S_{12}[1 - (S_{12} + S/2) \\ &\quad \times (S_{11} - S/2)^{-1}]m^{1/2}) - S_{12}/(S_{11} - S/2)]/\alpha_p, \\ s_z(x,z) &= \textstyle\int \varepsilon_{zz}^{\rm tot}(x,z)\,{\rm d}z \\ &= \sum_p \varepsilon_p \cos(\alpha_p x)[[(C_{11} - C_{12})/C_{11}m^{1/2}] \\ &\quad \times (C_{11} + 2C_{12})(\{2/[\beta_p \sin(\gamma_p t) + \gamma_p \sinh(\beta_p t)]\} \\ &\quad \times \{u_p[\gamma_p \cosh(\beta_p z)\sin(\gamma_p z) + \beta_p \sinh(\beta_p z) \\ &\quad \times \cos(\gamma_p z)] + v_p[\beta_p \cosh(\beta_p z)\sin(\gamma_p z) \\ &\quad - \gamma_p \sinh(\beta_p z)\cos(\gamma_p z)]\}[1/(\beta_p^2 + \gamma_p^2)] \\ &\quad - [S_{11} - S/2 - (S_{12} + S/2)^2/(S_{11} \\ &\quad - S/2)]m^{1/2}z) + [(S_{12} + S/2)/(S_{11} - S/2)]z], \end{aligned} \tag{4}$$

where, for the pth Fourier component, we have

$$\begin{aligned} r_p &= -\{S_{11} - [S_{12}^2/(S_{11} - S/2)]\}[\beta_p \cosh(\beta_p t/2) \\ &\quad \times \sin(\gamma_p t/2) - \gamma_p \sinh(\beta_p t/2)\cos(\gamma_p t/2)] + S_{12}\{1 \\ &\quad - [(S_{12} + S/2)/(S_{11} - S/2)]\}[\beta_p \cosh(\beta_p t/2) \\ &\quad \times \sin(\gamma_p t/2) + \gamma_p \sinh(\beta_p t/2)\cos(\gamma_p t/2)]m^{1/2}, \\ s_p &= \{S_{11} - [S_{12}^2/(S_{11} - S/2)]\}[\beta_p \sinh(\beta_p t/2)\cos(\gamma_p t/2) \\ &\quad + \gamma_p \cosh(\beta_p t/2)\sin(\gamma_p t/2)] - S_{12}\{1 - [(S_{12} \\ &\quad + S/2)/(S_{11} - S/2)]\}[\beta_p \sinh(\beta_p t/2)\cos(\gamma_p t/2) \\ &\quad - \gamma_p \cosh(\beta_p t/2)\sin(\gamma_p t/2)]m^{1/2}, \\ u_p &= -S_{12}\{1 - [(S_{12} + S/2)/(S_{11} - S/2)]\} \\ &\quad \times [\beta_p \cosh(\beta_p t/2)\sin(\gamma_p t/2) - \gamma_p \sinh(\beta_p t/2) \\ &\quad \times \cos(\gamma_p t/2)] + \{S_{11} - S/2 - [(S_{12} + S/2)^2 \\ &\quad \times (S_{11} - S/2)^{-1}]\}[\beta_p \cosh(\beta_p t/2)\sin(\gamma_p t/2) \\ &\quad + \gamma_p \sinh(\beta_p t/2)\cos(\gamma_p t/2)]m^{1/2}, \\ v_p &= S_{12}\{1 - [(S_{12} + S/2)/(S_{11} - S/2)]\}[\beta_p \sinh(\beta_p t/2) \\ &\quad \times \cos(\gamma_p t/2) + \gamma_p \cosh(\beta_p t/2)\sin(\gamma_p t/2)] \\ &\quad - \{S_{11} - S/2 - [(S_{12} + S/2)^2/(S_{11} - S/2)]\} \\ &\quad \times [\beta_p \sinh(\beta_p t/2)\cos(\gamma_p t/2) - \gamma_p \cosh(\beta_p t/2) \\ &\quad \times \sin(\gamma_p t/2)]m^{1/2}. \end{aligned} \tag{5}$$

Note that (4) and (5) hold in the case of finite size along the [011] crystallographic direction. Nevertheless, the same equations after straightforward modifications can give the atomic displacement components also in the case of finite size along the [001] crystallographic direction, *i.e.* when $\mathbf{x} = [100]$, $\mathbf{y} = [010]$ and $\mathbf{z} = [001]$. In order to do this, it is sufficient to put into (4) and (5) the values $m = 1$ and $n = 2(\alpha - \nu)/(1 - \nu)$ valid for this thinning direction, and to put $S = 0$ (instead of $S = S_{11} - S_{12} - S_{44}/2$) to avoid the rotation of axes needed for the thinning direction $\mathbf{z} = [011]/2^{1/2}$ but not for $\mathbf{z} = [001]$ (De Caro, Giuffrida & Tapfer, 1996).

Equations (4) and (5) were used to realize the supercell models of the distorted structures needed for HRTEM simulations (De Caro, Giuffrida, Carlino & Tapfer, 1995). In this respect, it is important to note that in the presence of non-uniform strain fields the supercells can contain thousands of atoms. Consequently, the use of a computer program for generating the model of the deformed structure, used in the HREM simulations, cannot be avoided (De Caro, Giuffrida, Carlino & Tapfer, 1995).

3. Results and discussion

3.1. *Lattice deformation and atomic displacement*

The strain field in the thinned strained heterostructures and the displaced atomic positions in the presence of elastic relaxation were calculated by implementing a computer program by the software *Mathematica* (Wolfram Research Inc., Champaign, Illinois, USA) running on an IBM RISC 6000 model 560 workstation. The format used for the files containing the coordinates of the atomic positions, *i.e.* the input data for making the supercell of the distorted structures, was chosen to be compatible with the Cerius-HRTEM software package (Molecular Simulation Inc., Cambridge, England), used for HRTEM image simulations. The HRTEM image simulations were performed on an IBM RISC 600 model 350 workstation equipped with a graphic card Sabine 24 bit.

Fig. 2 shows the non-uniform lattice deformation [(4)] due to the elastic relaxation phenomena in a GaAs/InAs superlattice period. In this case, we considered the following values of the geometrical parameters: $a = 11.3$, $b = 0.6$ and $t = 10$ nm. The arrows are the atomic displacement vectors with respect to the undeformed position (GaAs reference lattice), magnified by a factor of 2. Fig. 2 clearly shows that the atomic positions along the z axis lose their translational symmetry, contrary to the bulk situation of a tetragonal lattice distortion. Along the x axis, the superlattice periodicity of period $T = a + b$ remains unchanged, and only along the y axis does the lattice keep its original translational symmetry. Therefore, the supercell for the distorted heterostructure in the presence of

elastic relaxation must have the following dimensions: T along the x axis; t along the z axis and a unit cell along the y axis. As T and t are equal to several times the unit-cell dimension, we need to generate a supercell containing thousands of atoms by means of a computer program (De Caro, Giuffrida, Carlino & Tapfer, 1995).

From (1) also the averaged strain components can be obtained. In particular,

$$[\varepsilon_{xx}(x)]_{\rm ave} \equiv (1/t) \int_{-t/2}^{t/2} \varepsilon_{xx}^{\rm tot}(x, z)\, {\rm d}z = (1/t)[s_x(x, t/2) - s_x(x, -t/2)] \qquad (6)$$

gives the strain in the x direction, averaged along the z direction of finite size t as a function of the x coordinate. Since the z direction coincides with the zone axis along which the TEM observations are performed, the quantity given by (1) can be thought of as the average total strain of the column of atoms at the x position whose projected potential contributes to the HRTEM image contrast. In other words, we can define the average total strain $(\varepsilon_{xx})_{\rm ave}$ as the 'projected' total strain at the x position, in the sense of mean total strain of the atoms constituting the column at the x coordinate.

Fig. 3 shows the averaged strain $(\varepsilon_{xx})_{\rm ave}$ normalized with respect to the corresponding tetragonal value $(\varepsilon_{xx})_{\rm bulk}$ in the absence of elastic relaxation in the $In_{0.2}Ga_{0.8}As$ layer of a $GaAs/In_{0.2}Ga_{0.8}As$ superlattice, with the geometrical parameters $a = 9$, $b = 2.3$ and $T = 11.3$ nm. Different thickness values t and different thinning directions $\mathbf{z} = [011]/2^{1/2}$ and $\mathbf{z} = [001]$ were considered. Let us note that the ratio $(\varepsilon_{xx})_{\rm ave}/(\varepsilon_{xx})_{\rm bulk}$ does not depend on the lattice mismatch value but indirectly depends on the mole fraction through the variation of the stiffness constants as a function of the chemical composition. From Fig. 3, it can be deduced that when the t/T ratio reaches a value of 5 the strain value $(\varepsilon_{xx})_{\rm ave}$ of the thinned heterostructure is equal to about the 96% of that of the bulk heterostructure. The difference of about 4% multiplied by the actual strain value gives the possibility of evaluating whether the effect of elastic relaxation influences the average positions of the atoms in such a way to be visible experimentally. For example, with the assumption of an experimental accuracy of about 0.2% in the determination of the atomic column positions (Seitz, Seibt, Baumann, Ahlborn & Schoter, 1995), for $t/T = 5$, only a lattice mismatch greater than 5% may generate relaxation effects experimentally observable by analyzing the atomic column positions in the HRTEM image. On the other hand, from Fig. 3 it follows that for $t/T = 0.2$ even lattice mismatches of the order of 0.3% may generate elastic relaxation effects affecting the atomic column positions in the HRTEM images above the experimental accuracy. Thus, a GaAs/InGaAs superlattice with an InAs mole fraction $x = 0.2$ would give experimentally visible relaxation effects on the atomic column positions only for a particular range of t/T values. Analogous considerations hold for any other InAs mole fraction and for any other semiconductor heterostructure. Furthermore, from Fig. 3 it follows that the total strains of the

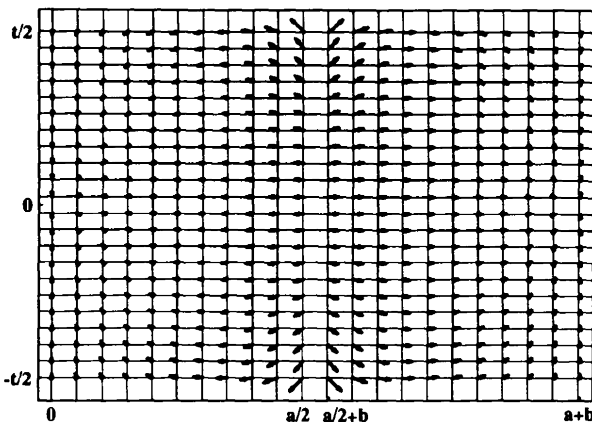

Fig. 2. Total atomic displacement field in the (x, z) plane for an elastically relaxed GaAs/InAs superlattice with period $T = 11.9$, $a_{\rm GaAs} = 11.3$, $b_{\rm InAs} = 0.6$ nm, and thickness $t = 10$ nm. The arrows are the atomic displacement vectors with respect to the undeformed positions (GaAs reference lattice), magnified by a fixed arbitrary factor.

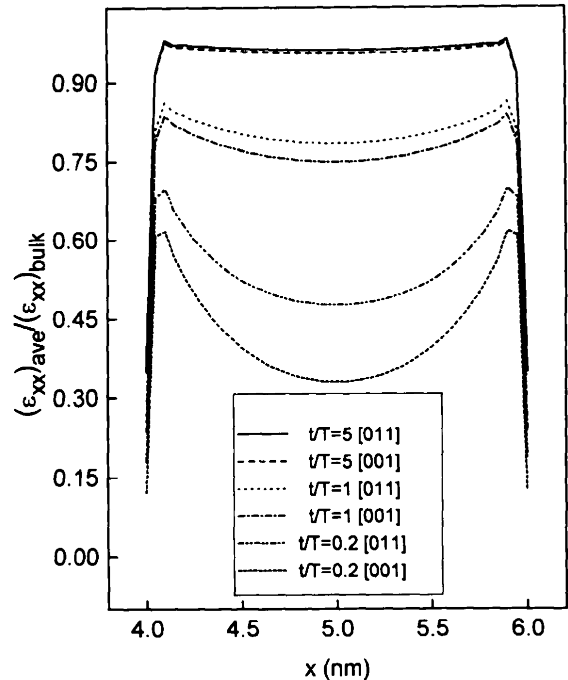

Fig. 3. Averaged strain $(\varepsilon_{xx})_{\rm ave}$ of equation (1), normalized with respect to the corresponding tetragonal value in the absence of elastic relaxation $(\varepsilon_{xx})_{\rm bulk}$ as a function of the x coordinate in the InGaAs layer of a $GaAs/In_{0.2}Ga_{0.8}As$ superlattice. $a = 9$, $b = 2.3$ and $T = 11.3$ nm. Different t/T ratios and thinning directions have been considered.

elastically relaxed structure can show a 15% variation as a function of the thinning direction, which is above the experimental accuracy. This finding invalidates the assumption made by other authors (Jouneau, Tardot, Feuillet, Mariette & Cibert, 1994) on the negligible influence of the thinning direction on the strain value of the elastically relaxed structure. In particular, in the limit $t/T \rightarrow 0$, the elastic strain value of $(1+\nu)\varepsilon_r$ is approached only when $\mathbf{z}=[001]$, where ε_r is the lattice mismatch. Otherwise, if $\mathbf{z}=[011]/2^{1/2}$, the strain value of $\{2\alpha(1+\nu)/[\alpha(1+\nu)+1-\nu]\}\varepsilon_r$ is approached (De Caro & Tapfer, 1994). Obviously, only for an isotropic medium ($\alpha = 1$) do we obtain the same limit value for any z direction again.

Let us note that in Fig. 3 we discussed the dependence of $(\varepsilon_{xx})_{\rm ave}/(\varepsilon_{xx})_{\rm bulk}$ as a function of the t/T ratio, but not as a function of the different values of t or T. In fact, as first pointed out by Treacy, Gibson & Howie (1985), the extent of the elastic relaxation depends on the t/T ratio only. This is shown in Fig. 4, where $(\varepsilon_{xx})_{\rm ave}/(\varepsilon_{xx})_{\rm bulk}$ in the center ($x = T/2$, $z = 0$) of an $In_{0.2}Ga_{0.8}As$ layer of a GaAs/$In_{0.2}Ga_{0.8}As$ superlattice is considered as a function of the specimen thickness t. The b/a ratio was kept constant ($= 1/4$) and different T values were considered. If we join the points of different curves corresponding to the same value of t/T, we obtain horizontal lines (the solid line in Fig. 4 corresponds to $t/T = 4$). This finding directly confirms the results reported by Treacy, Gibson & Howie (1985). Furthermore, from Fig. 4, it can be deduced that the minimum value of $(\varepsilon_{xx})_{\rm ave}/(\varepsilon_{xx})_{\rm bulk}$ is not reached for $t/T = 0$. In fact, the curves of Fig. 4 show a minimum near the value $t/T = 0.16$, which is particularly evidenced for the curve obtained for $T = 100$ nm (better resolution in the neighborhood of $t/T = 0.16$). This finding is related to the anisotropic properties of the crystalline structure. In fact, with $\alpha = 1$, the minimum is reached at $t/T = 0$.

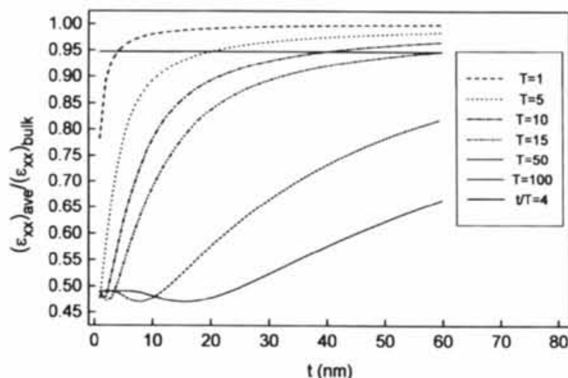

Fig. 4. $(\varepsilon_{xx})_{\rm ave}/(\varepsilon_{xx})_{\rm bulk}$ in the center ($x = T/2$, $z = 0$) of an $In_{0.2}Ga_{0.8}As$ layer of a GaAs/$In_{0.2}Ga_{0.8}As$ superlattice as a function of the specimen thickness t, for different T values. The b/a ratio was fixed at 1/4 for all the curves.

3.2. *HREM image simulations*

Fig. 5 shows the HRTEM simulated images in the [011]-zone axis for 2 monolayers of InAs buried in a GaAs matrix. Fig. 5(*a*) has been obtained for a tetragonal lattice distortion, whereas Fig. 5(*b*) has been obtained taking into account the elastic relaxation contribution. We have put $a \gg b$ in our calculations, where a and b are the thicknesses of the GaAs and InAs materials, respectively. The corresponding displacement vector field is reported in Fig. 2. The values of the electro-optical parameters used in the simulations are: electron energy = 400 kV, spherical aberration coefficient = 1.8 mm, defocus spread = 8 nm, defocus = 0 nm, beam divergence = 0.8 mrad, objective-lens radius $\equiv R_{\rm ol} = 6$ nm^{-1}. The thickness of the specimen is 10 nm. The number of Fourier components used in the simulations were calculated by imposing

$$(2\pi p_{\rm max}/T) \leq R_{\rm ol}. \quad (7)$$

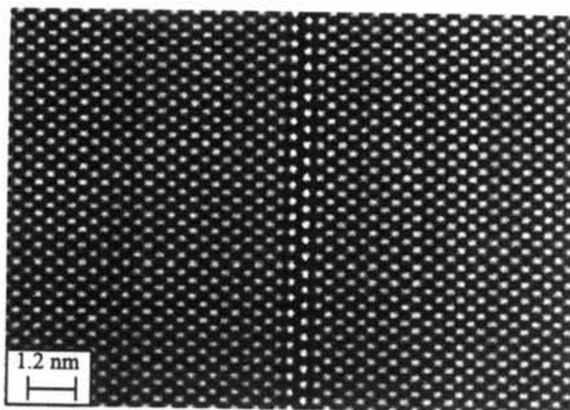

(*a*)

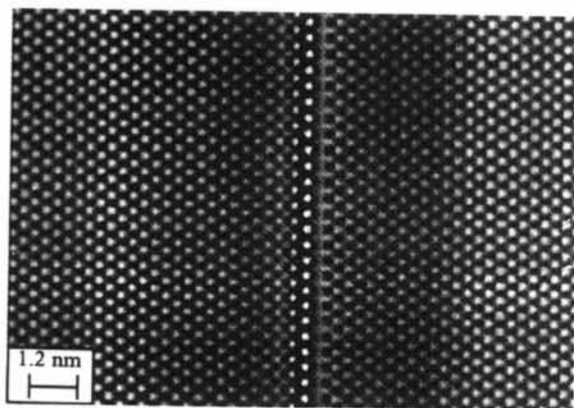

(*b*)

Fig. 5. HRTEM simulated images for two InAs monolayers buried in a GaAs matrix: (*a*) with a tetragonal lattice deformation; (*b*) by considering elastic relaxation effects. For the parameter values used in the simulation, see text.

In fact, we verified that even by considering many more Fourier components than the p_{max} calculated by using (7), with frequencies higher than those permitted by the objective-lens aperture, the peculiar features of the obtained HRTEM simulations remain unchanged.

As shown in Fig. 5(*b*), the elastic relaxation generates a contrast gradient in the image, which extends several ångströms from the heterointerface and which is absent in the case of a pure tetragonal deformation (Fig. 5*a*). This background intensity variation generated by the bending of the atomic columns (see Fig. 2) is present for large ranges of defocus values and specimen thicknesses. It is worthwhile mentioning that the simulated image contrast near the strained heterointerfaces in Fig. 5(*b*) was observed experimentally by Bierwolf, Hohenstein, Phillipp, Brandt, Crook & Ploog (1993) for a few monolayers of InAs buried in a GaAs matrix. If the elastic relaxation effects are neglected, the above background-intensity variation could be erroneously interpreted as due to the diffusion of indium in the GaAs matrix.

Fig. 6 shows the HRTEM simulated images in the [011]-zone axis for 2 monolayers of Ge buried in an Si matrix. Fig. 6(*a*) has been obtained for a tetragonal lattice distortion, whereas Fig. 6(*b*) has been obtained taking into account the elastic relaxation contribution. The values of the electro-optical parameters and the specimen thickness used in the simulations are the same as in Fig. 5. It is interesting to note the absence of any contrast gradient in both Figs. 6(*a*) and (*b*). The same result is obtained for any defocus value and specimen thickness. Moreover, we have also substituted in the supercell realized for obtaining Fig. 5(*b*) the atoms of the InAs layer with Ge atoms and the atoms of the GaAs matrix with Si atoms. In this way, we have artificially generated an Si/Ge heterostructure with a diamond-like structure and a lattice mismatch of 7%. Nevertheless, no background intensity variation was in evidence. The above results imply that the information on the contrast gradient in the HRTEM images, owing to the non-uniform lattice distortion of an elastically relaxed heterostructure made by cubic materials, is contained in the {200} beams, forbidden for diamond-like crystallographic structures.

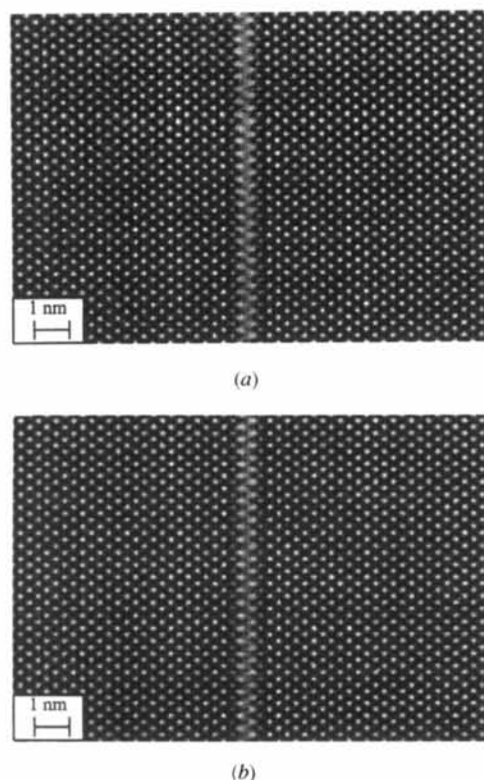

Fig. 6. HRTEM simulated images for two Ge monolayers buried in an Si matrix: (*a*) with a tetragonal lattice deformation; (*b*) by considering elastic relaxation effects. For the parameter values used in the simulation, see text.

In fact, since the strongest lattice deformation gradient occurs perpendicular to the heterointerfaces, the points in the reciprocal space perpendicular to the heterointerfaces should yield the maximum information on the deformation field. The same happens for the {200} beams that are perpendicular to the heterointerface for both the [100] and [011] thinning directions. This happens also for the {400} beams, which, however, are at higher frequencies than the {200} beams. Consequently, they should only contain information on high-order components of the Fourier series given by (4), whose corresponding amplitudes are very small. Moreover, from an experimental point of view, the {400} beams are cut off either by the damping envelope or the objective-lens aperture of most of the existing transmission electron microscopes. Therefore, if {200} beams are forbidden for cubic materials (diamond structure), no detectable background-intensity variation should be expected. On the contrary, for all the III–V and II–VI compounds with zinc blende structure, the background-intensity variation should always be present and it should be proportional to the lattice mismatch value and to the difference between the atomic scattering factors of the two atomic species involved.

4. Conclusions

In this work, we investigated the effects of the elastic relaxation of compositional stresses due to the thinning of TEM specimens on the image contrast of HRTEM micrographs of strained heterostructures made by cubic materials. In particular, TEM specimens of strained semiconductor materials with zinc blende crystallographic structure produce HRTEM images showing a strong contrast gradient. This effect is due

to the non-uniform lattice deformations caused by the elastic relaxation phenomena. This kind of image contrast could also be generated by other physical phenomena, for example chemical diffusion. For this reason, the possible influence of the elastic relaxation on the image contrast has to be taken into account.

On the other hand, TEM thinned specimens of strained semiconductor materials with diamond crystallographic structure (*e.g.* 2 monolayers of Ge buried in an Si matrix) lead to no contrast gradients in the HRTEM images. This finding indicates how the information due to the non-uniform lattice distortion of an elastically relaxed heterostructure made by materials with a cubic crystallographic symmetry is contained in the {200} beams, forbidden for diamond-like crystallographic structures.

Our results also show that the total strains of an elastically relaxed structure can vary by up to 15% as a function of the thinning direction ([100] or [011]), which, therefore, is a fundamental parameter in the strain status modeling of TEM specimens.

The strain fields obtained for finite-size strained heterostructures are very different from those obtained for the bulk ones. Therefore, the influence of elastic relaxation cannot be neglected whenever HRTEM is used to deduce the local chemical composition or the local unit cell in strained cubic materials.

References

Bierwolf, R., Hohenstein, M., Phillipp, F., Brandt, O., Crook, G. E. & Ploog, K. (1993). *Ultramicroscopy*, **49**, 273–285.

De Caro, L., Giuffrida, A., Carlino, E. & Tapfer, L. (1995). *Microsc. Microanal. Microstruct.* **6**, 465–472.

De Caro, L., Giuffrida, A. & Tapfer, L. (1996). *Phys. Rev.* **B54**, 10575–10584.

De Caro, L. & Tapfer, L. (1994). *Phys. Rev. B*, **49**, 11127–11133.

Gibson, J. M. & Treacy, M. M. J. (1984). *Ultramicroscopy*, **14**, 345–350.

Hybertsen, M. (1990). *Phys. Rev. Lett.* **64**, 555–558.

Hybertsen, M. (1991). *Appl. Phys. Lett.* **58**, 1759–1761.

Jouneau, P. H., Tardot, A., Feuillet, G., Mariette, H. & Cibert, J. (1994). *J. Appl. Phys.* **75**, 7310–7316.

Perovic, D. D., Weatherly, G. C. & Houghton, D. C. (1988). *J. Vac. Sci. Technol.* A**6**, 1333–1336.

Perovic, D. D., Weatherly, G. C. & Houghton, D. C. (1991). *Philos. Mag.* A**64**, 1–13.

Seitz, H., Seibt, M., Baumann, F. H., Ahlborn, K. & Schoter, W. (1995). *Phys. Status Solidi*, **150**, 625–632.

Spence, J. C. H. (1981). *Experimental High Resolution Electron Microscopy*. Oxford: Clarendon.

Treacy, M. M. J. & Gibson, J. M. (1986). *J. Vac. Sci. Technol.* B**4**, 1458–1466.

Treacy, M. M. J., Gibson, J. M. & Howie, A. (1985). *Philos. Mag.* A**51**, 389–417.

Vandenberg, J. M., Macrander, A. T., Hamm, R. A. & Panish, M. B. (1991). *Phys. Rev. B*, **44**, 3391–3394.